ETH
Eidgenössische Technische Hochschule Zürich
Swiss Federal Institute of Technology Zurich

Institut für Integrierte Systeme
Integrated Systems Laboratory

Department of Information Technology and
Electrical Engineering

Spring Semester 2021

UWB for micro-drones

Bachelor Project

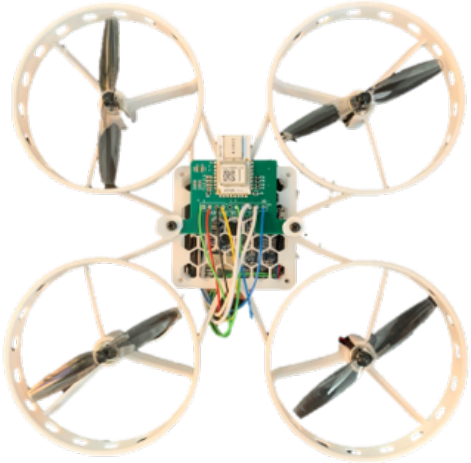

Yanick Büchel
ybuechel@student.ethz.ch

June 11th 2021

Supervisors: Dr. Tommaso Polonelli, tommaso.polonelli@pbl.ee.ethz.ch
Dr. Michele Magno, michele.magno@pbl.ee.ethz.ch
Professor: Prof. Dr. L. Benini, lbenini@iis.ee.ethz.ch

Acknowledgements

At this point, I would like to express a special thanks to both my supervisors, Dr. Tommaso Polonelli and Dr. Michele Magno, who even in times of the Pandemic and Social Distancing accompanied and supported me in weekly online and in person meetings with informative inputs and understandable answers to all my questions.
I also want to thank Prof. Dr. Luca Benini for letting me work on my thesis at his department.

Abstract

Knowing the exact position of a drone is a key parameter when it comes to it acting autonomously in space. In Global Navigation Satellite System (GNSS) denied environments, alternatives are needed for indoor navigation. At this point, Ultra-Wideband (UWB) technology offers a cost-effective and energy-efficient solution.
Using Two-Way ranging (TWR), the distance to anchor points can be estimated with an average resolution of 10 cm, enough to enable indoor navigation. With at least four anchor points, the position in space can then be calculated using multilateration.
With the 'DWM1000' UWB module, there are already implementations that make use of this technology, see [1] and [2].
With the successor, the 'DWM3000', there are to current knowledge still no comparable systems. On that account, this thesis deals with the study and evaluation of UWB technology, getting to know the DWM3000 module and the exploration of the 'Steval-Drone01' micro-drone kit that does not feature any native navigation technology. Subsequently, the gathered knowledge is combined to design a printed circuit board (PCB) for the micro-drone that implements the DWM3000. Furthermore, a software for the flight control unit (FCU) of the drone is used to test its functionality.

Declaration of Originality

I hereby confirm that I am the sole author of the written work here enclosed and that I have compiled it in my own words. Parts excepted are corrections of form and content by the supervisor. For a detailed version of the declaration of originality, please refer to Appendix C.

Yanick Büchel,
Zurich, June 11th 2021

Contents

Chapter 1

Introduction

Although drones might still have more of a hobbyist reputation these days, they are becoming an increasingly important piece of the IoT infrastructure puzzle. The industry sees huge potential in these Unmanned Aerial Vehicles (UAV). They push their development towards remarkable increases in computational capabilities and decreasing form factors.
A good example is Amazon founder Jeff Bezos who announced his company's autonomous drone delivery system to CBS's TV show "60 Minutes" in 2013. On the question how long it would take until the drones are operational, he replied:
"I'm an optimist... could it be four, five years? I think so. It will work, and it will happen, and it's gonna be a lot of fun." [3]

While pioneering research has already demonstrated nano-scale UAVs, i.e. micro-size drones, these form factors do in general not allow flight control, navigation or planning capabilities and if, they are based on monocular cameras. Reasons are that the payload of a micro-drone is limited to a few grams and that additional sensor technology consume power from an already limited power budget.
Looking in the other direction towards relatively larger drones, namely DJI, Yuneec or Parrot, which have proven being capable of impressive sense-and-act capabilities, running complex machine learning algorithms in real-time using multi-sensor and vision-based inputs to control the flight. Drones have a wide variety of uses, such as building inspections (see [4]), express delivery of goods [5] (including medical supplies), high precision crop monitoring or research. In this project the focus lies on micro-sized UAVs, typically having a few centimeters in diameter and only tens of grams in weight. As a consequence, they only have a few watts of total power consumption of which 85 % is dedicated to the motors, leaving a total power budget of only a few hundred mW.

The micro-size UAV in this project is based on the STEVAL-DRONE01 mini drone kit featuring the high performance STEVAL-FCU001V1 flight controller unit, which supports custom firmware and hardware.

1.1. Contribution

The goal of this work is adding the capability of indoor real-time locating to the Steval-DRONE01 micro-drone. While in general indoor positioning via global navigation satellite systems (GNSS) e.g. GPS fails inside multistory buildings, there already exist solutions leveraging the existence of WiFi networks, reaching accuracies of up to 5 m by implementing received signal strength indicators (RSSI) [6]. Alternatively, it is possible to reach up to 1 m precise measurements with the BLE standard [7]. However, what these solutions have in common is their accuracy in the scale of a few meters such that it is not feasible for precise tracking within tens of centimeters. In contrast, UWB technology offers ranging accuracies of less than 10 cm [8].

This thesis focuses on enhancing the micro-drones capabilities by adding indoor positioning through the DWM3000, the state-of-the-art Ultra-Wideband (UWB) transceiver. Specifically, this means that a custom design of a printed circuit board (PCB) is developed. This PCB allows for connection between the flight control unit (FCU) and the DWM3000.

The work includes the study of UWB ranging and the DWM3000 itself, STM32 programming the PCB Design with Altium Designer. Because of the small form factor of the drone and therefore the limited power budget, the focus lies on a power efficient PCB that is feasible for the use with micro-drones. The work is structured into three phases, refer to Appendix A for the detailed Task Description.

1.2. Thesis Organization

The present work is organized as follows. Succeeding this introductory chapter, Chapter 2 addresses the theoretical background regarding UWB sensors and their working principle. This is followed by a brief introduction to UAVs and PCBs. The end of this chapter is dedicated to related work that has been done in this area.
Chapter 3 covers the Hardware and Software Implementation by firstly giving a detailed overview of the FCU and the UWB module (HW and SW). Followed by section 3.3 that describes the PCB design and its process.
The Results are presented in Chapter 4 which is followed by Chapter 5 where the work is concluded.

Chapter 2

Background and State of the Art

2.1. UWB

In general, an UWB signal is defined to be a signal with a fractional bandwidth of larger than 0.2 for UWB systems with a center frequency f_c lower than 2.5 GHz and for systems with f_c larger than 2.5 GHz the bandwidth has to be at least 500 MHz [9]. The ultra wide bandwidth comes from the nature of the channel impulse responses of the signal and vice versa. Narrow signals have a broad frequency spectrum (Fourier Signal Analysis). Due to these sharp pulses of the UWB signal, the transceivers of such a system can resolve individual multipath components (MPCs) and hence are capable of accurately estimating the time of arrival of the first signal path. This results in high resolution channel impulse response estimation and accurate time of flight measurements between a transmitter and a receiver [10][11]. While the precise distance estimation might be one of the most popular aspects of the UWB technology, there are other important advantages:

- penetration through obstacles[9]
- high-speed data communications[9]
- low cost and low power implementations[9]

The good penetration capability is due to the fact that the frequency spectrum of the system includes both high and low frequencies.
Regarding the last aspect; an UWB system can be operated carrier-free[1]. This reduces the need of signal processing, which makes lower cost implementations possible[9].

[1] a pulse is transmitted without a sine-wave carrier

2.1.1. Distance Estimation Techniques

In recent years, vision-based control inspired research efforts in UAVs; making possible complex, yet precise flight maneuvers [12]. Nonetheless, these performances rely on a complex and expensive motion capture system. Cost-efficient and already established indoor positioning systems based on BLE and Wifi [7][6] however, cannot provide high enough accuracy. The need for a low-cost implementation of an indoor positioning system is met by UWB systems. UWB offers precise ranging at relatively low cost. As a first step to estimate a position, a set of position-related parameters have to be estimated. For this purpose, the following methods exist and are explained in this section [13].

- Time of Arrival (ToA)
- Time Difference of Arrival (TDoA)
- Received Signal Strength (RSS)
- Angle of Arrival (AoA)

The first two rely on precise time stamping, the ToA methods further involve single-sided TWR, double-sided TWR. In this section the techniques are described in the above order.

Time of Arrival/Two-way ranging (TWR)

In radio technology, the concept of two way ranging (TWR) is used to determine the distance between two objects by measuring the time of flight (ToF) of the signals between them. The distance is calculated via the formula,

$$Distance = Speed\,of\,radio\,waves \cdot ToF \tag{2.1}$$

"TWR has advantages over other distance measurement and locating systems in that it can be used by stand-alone devices which only have relative distances to measure. There is no requirement for an infrastructure of fixed communicating devices to determine separation distances" [14].

Single-sided TWR

The key concept of a TWR exchange is depicted in Figure 2.1. The two vertical axes represent the time of Device A and B respectively. Note that these times rely on the devices' independent, unsynchronized clocks.
The ranging procedure starts when device A is sending a message to B, visualized by the arrow from left to right. The moment the message leaves A's antenna, A sets a timestamp. Another timestamp is set when the reply message from B arrives at A's antenna.

From B's perspective, the following happens. As soon as A's message arrives at its antenna, B computes a response message, containing the timestamps from reception of the first message from A and transmission of the reply. From this, the response delay of B, denoted as T_{replyB}, can be calculated. Note that the interrupted vertical lines should indicate that the reply times are usually a lot longer than the ToF of the signals[2]. The time-of-flight, T_f, is in the range of a few nanoseconds since $d = c \cdot T_f$ is already 0.3 m for T_f=1 ns.
To get T_f from the described exchange, one can derive from Figure 2.1 the equation $T_{roundtripA} = 2 \times T_f + T_{replyB}$. This is equal to:

$$T_f = \frac{T_{roundtripA} - T_{replyB}}{2} \tag{2.2}$$

However, due to clock drift [3] in both device's clocks, there are inevitable timing errors, and thus errors introduced to the distance estimation. A method to reduce this error is double-sided TWR.

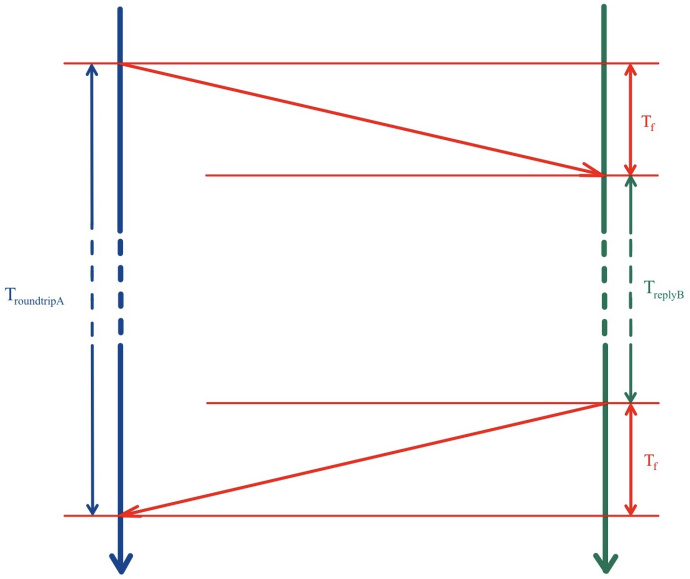

Figure 2.1.: Single-sided TWR exchange

[2] reply time in the μs range whereas the the latter is in the ns range
[3] due to crystal imperfections

Double-sided TWR

Double-sided TWR is a modification of the single-sided TWR and counteracts the fact that the two devices have different clock frequencies due to crystal imperfections. It improves accuracy even for long response delays by performing two single-sided TWR exchanges. In this section the double sided TWR with three messages (also referred to as asymmetric double-sided TWR) is discussed. This concept is depicted in Figure 2.2. The double-sided TWR exchange starts as a single-sided TWR exchange. However, by responding to device A, device B initiates its own roundtrip measurement. This means that the reception of B's response at device A triggers an additional message from A containing information about A's response delay T_{replyA}. The time of flight T_f can then be calculated as

$$T_f = \frac{T_{roundtripA} \cdot T_{roundtripB} - T_{replyA} \cdot T_{replyB}}{T_{roundtripA} + T_{roundtripB} + T_{replyA} + T_{replyB}} \tag{2.3}$$

Time Difference of Arrival

In measuring the time difference of arrival (TDoA) of a signal, the target node is localized based on different arrival times at multiple fixed nodes with known position. The signal leaves the target nodes' antenna at time t_0. From the different arrival times t_n at nodes n for $n = 1, 2, 3, ...$, the position of the target can be computed. It is very important that the fixed nodes, anchors, have synchronized clocks such that the arrival times can be compared. The synchronization can either be handled by a so called "coordinator" that sends periodic blinks to the anchors or wiring all anchors with a common clock [15].

Received Signal Strength

The received signal strength method (RSS) leverages known channel-characteristics, such as the relation between distance and power loss of the signal to infer the distance to its transmitter. The accuracy is rather poor compared to UWB methods[16].

2.1.2. Other methods

Angle of Arrival

Generally, the angle of arrival of a signal is detected by employing antenna arrays. The antennas measure the TDoA and with known antenna separation l, the angle to the sender can be inferred. If the distance between the sender and receiver is large enough, the incoming signal can be modeled as a planar wave[4]. The difference of arrival times

[4] farfield approximation

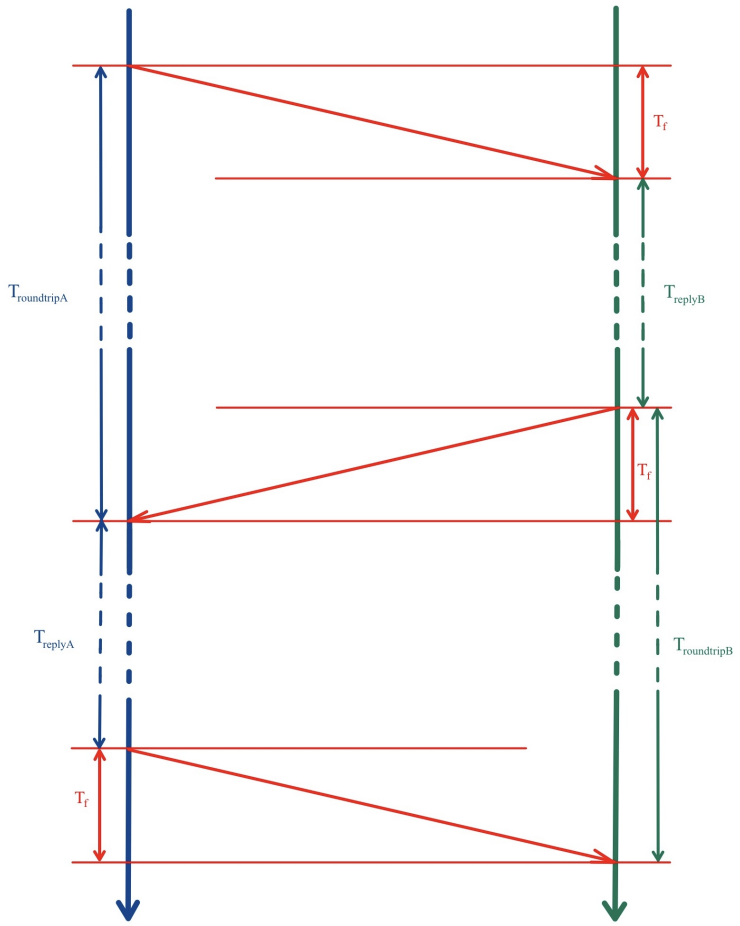

Figure 2.2.: Double-sided TWR exchange. Also refer to Figure 4.1 in Section 4.1 and note the three peaks indicating poll, response and final frame of TWR exchange

then is approximately $l \cdot \frac{\sin \phi}{c}$, see Figure 2.3. From this it is possible to determine the phase differences of arrival and consequently extract angle information[13].

2.1.3. DWM3000 based TWR

The DWM3000 uses the DS-TWR method described in Section 2.1.1. In the dialect of the manufacturer the exchange consists of a so called “poll”, “response” and “final” frame, corresponding to the first, second and third message exchanged between the two devices.

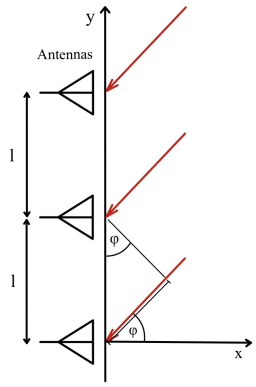

Figure 2.3.: AoA Method

2.2. UAV Drones

An unmanned aerial vehicle (UAV), also referred to as drone, is as its name suggests an aircraft without a human pilot; instead the UAV is controlled from a ground operator. Nowadays, UAVs come in all different forms and sizes, however in this work we are focussing on quadcopters - a multicopter with four rotors.
As one can see from Figure 2.4, drones can be divided into three main segments; there are toy/micro drones, consumer drones and drones used for industrial applications. While for a micro-drone DC brushed motors with a simple speed controller and a flight controller suffices, going towards larger consumer and industrial drones, more expensive brushless DC motors are commonly required together with GPS capability, gimbal control and other sensors. Consequently, going from the sparsely equipped micro drones towards the highly capable Industrial drones, the price increases, starting in the range of tens of dollars towards the range of thousands of dollars.

In the following, the main components of a quadcopter are being described.

Frame

The frame is the most noticeable component of a drone. It forms the basic structure of the UAV, which holds all other components together. Size, weight and the frame structure itself are the key factors one has to consider. However, depending on the application, there are other aspects to consider. One could be the choice of material where for example Carbon offers suitable physical properties such as light weight and high stiffness; on the other hand, the material is not very RF-transparent. Antennas must therefore be placed with consideration.

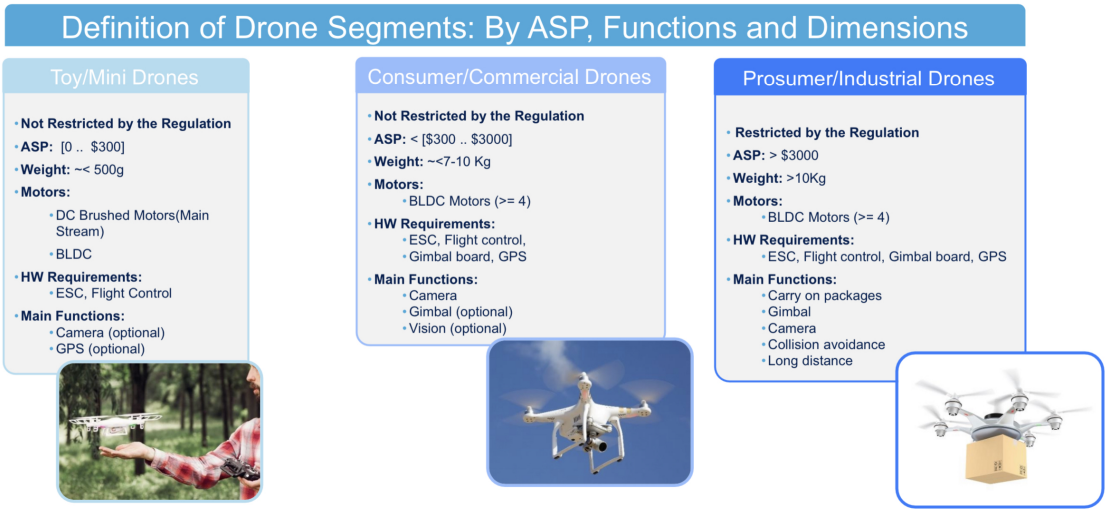

Figure 2.4.: Drone categories [17]

Flight Control Unit (FCU)

This is the center piece of the drone. It is equipped with sensors such as a 3D accelerometer, 3D gyropscope[5], magnetometer and pressure sensor on top, such that the FCU can estimate the UAVs current state of flight precisely. Using PID controllers it computes the thrust required from each motor such that the control input from the ground is translated to the actual flight. Therefore it needs to have a radio receiver connected, and also an ESC to drive the motors. Even though the FCU001V1 that is used in this project, has built in power distribution system, ESC and a BLE module for connectivity; these components are being introduced separately in the following.

Power Distribution Board

Usually, this components is directly connected to the battery. It has a wide input voltage range and transforms it to a stable output voltage to power other components, i.e. FCU. Many FCUs offer an all-in-one package with this components already onboard.

Battery

Drones are commonly fueled by LiPo[6] batteries, they offer high energy densities and are able to deliver large amount of power. Each LiPo cell has a nominal voltage of 3.7 V. If higher voltage is required, the cells can be connected in series. Typically, you do not

[5] accelerometer and gyroscope are usually combined in an Inertial Measurement Unit (IMU)
[6] LiPo stands for Lithium Polymer

refer to the battery voltage but the number of cells connected, or how many „S“ [18], see table 2.1.

symbol	no. cells	voltage [V]
1S	1 cell	3.7
2S	2 cells	7.4
3S	3 cells	11.1

Table 2.1.: LiPo Battery: cell count - voltage relation

Radio Receiver

The radio receiver is responsible for receiving the control inputs over the air and redirecting them to the FCU. Most receivers use Pulse-position modulation (PPM) or a digital serial protocol. The latter has the advantage that with only one wire, it is possible to control multiple channels. However, the range is typically a lot lower[7].

Electronic Speed Controller

An electronic speed controller (ESC) is a device that receives throttle signals from the flight controller. From there, it then drives the motors at the required speed.
An ESC provides four inputs of which two are the control signals of the FCU and the other two, usually thicker cables, are the power supply. Three output wires lead directly to the ones from a BLDC motor.

Motors

The motors consume the most power of all the components. The choice of motor highly depends on the size and weight of the drone. For micro drones, brushed motors are generally used. Due to the high power demand, an efficient combination of rotors and motors is necessary.

Rotors

On every quadcopter, there are two motors spinning CW and two CCW. For this reason, matching propellers are required as well as opposing direction of rotation, such that the angular velocity cancels out when hovering. In general, a heavier propeller requires more torque than a lighter propeller. Also blades with higher angle of attack create more drag

[7] below 100 m for both classic Bluetooth and BLE

and thus more torque. Since more torque means more current drawn by the motor it is important to find a feasible balance between generated thrust and the current the motor requires.

2.3. Printed Circuit Boards (PCB)

A printed circuit board (PCB) is a board that electrically connects electronic components with connections referred to as 'traces' or 'nets'. A modern PCB consists of multiple electrical layers, that allow more circuitry and wiring on the same area for more complex systems. The Stack-up of a PCB refers to the arrangement of copper layers and insulating layers that make up a PCB prior to board layout design. Another advantage of such a 'layer stack' is that it can help minimizing a circuit's vulnerability to external noise as well as minimize radiation and reduce impedance and crosstalk concerns on high-speed PCB layouts [19]. The layers can be electrically connected through 'vias'. Vias connecting the bottom layer to the top layer are called 'through hole', vias visible on only one side of the PCB are called 'blind' and vias that are not visible connecting internal layers are called 'buried'.
The PCB has "pads" which allow the components to be soldered to. The mounting of electronic components can be divided into two categories, the through-hole technology (THT) and the surface-mount technology (SMT). The main difference between the two is that SMT is handling way smaller form factors and is soldered directly to the surface of the pads whereas for SMT components holes have to be drilled into the PCB to insert the leads of the components. Depicted in Figure 2.5 is this works PCB shield as a design on the computer and the final assembly of it.

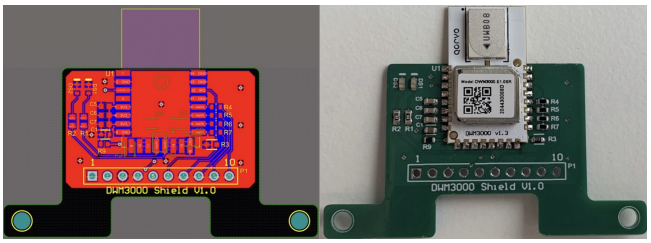

Figure 2.5.: This work's PCB design on Altium Designer (left) and realized as a board assembled with the components (right). The board is double sided, with through-hole plating, green solder mask and a white silkscreen.

2.4. Related Work

This section will provide a brief introduction to show what has already been achieved with UWB sensors, in particular the DWM1000, the predecessor of the DWM3000.

The authors of [2] proposed an ultra-wideband (UWB) positioning system, based on the DWM1000, whose position calculations are transformed to meet the existing navigation controller's implementations based on GNSS reception. Besides the first path detection that allows precise ToA reconstruction, they introduced the possibility of distinguishing between line-of-sight (LoS) and NLoS signals. This case distinction was based on a threshold for a new metric, the first path ratio.

The company bitcraze offers with its "Loco Positioning System" a local positioning system , based on the DWM1000, for their Crazyfly micro-drones. It implements TWR and TDoA methods. According to their website [1], a realistic number of anchors for accurate 3D localization is six in the TWR scenario.

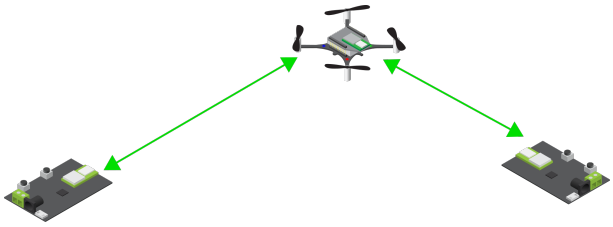

Figure 2.6.: Loco Positioning System by bitcraze [1]

In [16] the authors improved localization of remote targets. They did so by using a multi-stage navigation method that allows the UAV to autonomously fly to designated wireless sensor devices located at for humans inaccessible locations. In brief, the navigation works as follows. Via internally stored GPS coordinates of the target node, the drone gets in the proximity of around 10 m; from there a combination of UWB , ultrasonic and voltage sensors take over to enable localization in the sub-meter range.

Similarly at ETH Zürich, the group [20] introduces a low-power localization system to find and communicate with wireless sensor devices, whose location is not known a priori. The employed UWB system is based on the DWM1000 module and reaches an accuracy of less than 1 m while only requiring three measurements at different positions.

In [21] an autonomous multi-robot relative positioning technique using the DWM1000 is introduced and applied to a swarm of micro-drones. An Extended Kalman filter (EKF) uses sensing values of velocity, yaw rate, and height to then estimate the relative position of other robots by combining these quantities with on-board UWB ranging measurements.

Lastly, [8] and [22] investigated the performance of the Decawave DW1000 with Decawave's own evaluation kits . In [8], the authors made indoor and outdoor TWR mea-

surements with accuracies in the sub 10 cm range.

According to [22], 2D localization is possible in the sub-meter range, however for 3D localization, the accuracy in the z-axis still needs to be improved.

Chapter 3

Hardware and Software Implementation

This chapter describes how the final PCB shield was developed. Besides, it gives an introduction to the hardware and software platform for which the PCB was designed for. As a first step, an overview of the the FCU001V1, the drone's flight control unit, had to be created. Combining this knowledge with the study of the DWM3000 module, it was possible to work out the signals that the DWM3000 needed and where they can be connected physically on the FCU board.
Alongside, a firmware had to be written for the FCU001V1, the host controller for the DWM3000, to perform TWR measurements whilst not using any peripheral or signal that is used by the software that is controlling the flight.

3.1. The Drone Board - FCU001V1

Along with the STEVAL-FCU001V1 FCU from STMicroelectronics (STM), there is a complete sample firmware project, called STSW-FCU001, available which allows flying small or medium sized quadcopters out-of-the-box.
The FCU can be controlled by a standard external remote controller (over the PWM input interface) or by a smartphone or tablet through the on-board Bluetooth low energy module. Magnetometer and pressure sensors are embedded to support future 3D navigation applications.
SWD, I^2C ,UART and SPI[1] connectors are available for firmware development and debugging, and to support additional external sensors or RF modules, the connectors for the UART and I^2C are denoted as P7 and P3 in Figure 3.1 and 3.2. As being discussed in Section 3.3.1, a SPI connector is needed for the PCB shield.

[1]SPI is available after some hardware adjustments, see Section 3.3.1

3.1.1. FCU001V1 Hardware Description

The STEVAL-FCU001V1 evaluation board comes with a sample firmware project that allows flying small to medium sized quadcopters equipped with DC motors. For larger quadcopters, an external ESC can be used.
To control the board, the user can either choose BLE (smartphone or tablet) or a Remote Controller which therefore needs an RF receiver module at the PWM input, see connector P6 in Figures 3.1 and 3.2.
For the following description please follow along with Figure 3.1. Measuring 4 cm x 4 cm, the FCU contains an STM32F401 MCU as the main processing unit with 256 Kbytes of Flash memory and 64 Kbytes of RAM. Three sensors, namely a LSM6DSL inertial measurement unit (3D accelerometer and 3D gyroscope), a LIS2MDL high performance 3D magnetometer and a LPS22HD MEMS pressure sensor. For communication, a SPBTLE-RF module with integrated chip-antenna for BLE is available on the board. In terms of power there is a LD39015 voltage regulator installed that steps down the battery voltage to the 3.3 V required by the MCU and its peripherals. The battery itself can be charged directly when connected to the flight controller, which in turn must be connected to a micro USB cable. This is made possible by the on-board STC4054 800 mA Li-Ion battery charger.

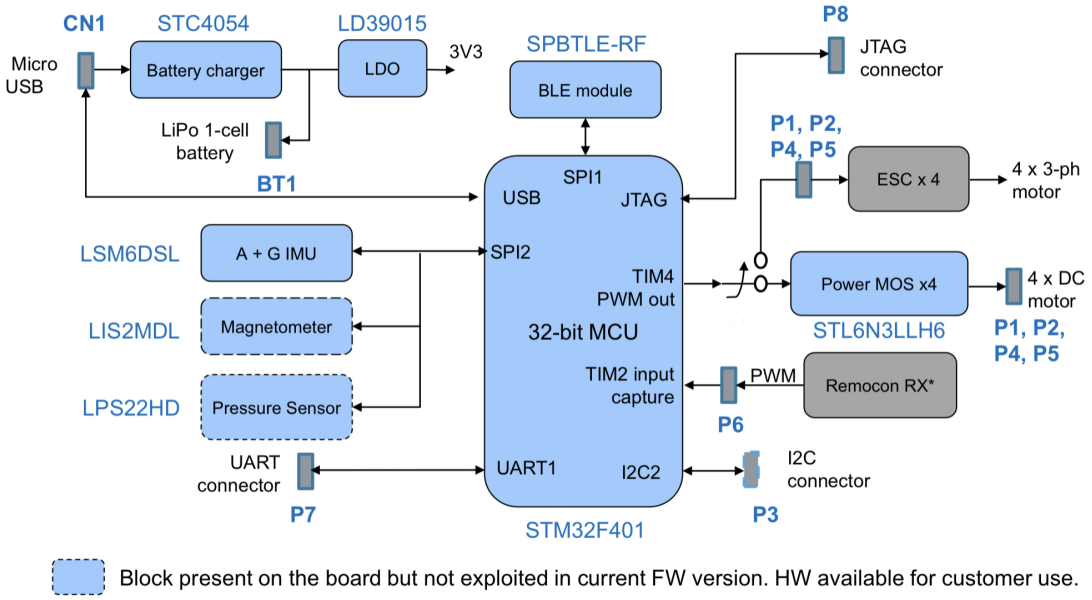

Figure 3.1.: FCU001V1 block diagram [17]

In Figure 3.3 are the STM32F401 connections[2]. The connections from the BLE, sensors and the motors are considered as fixed, they are internally connected to their corresponding peripheral; thus cannot be modified. Nevertheless, the R/C signals are not used in

[2]screenshot from the STM32CubeMX

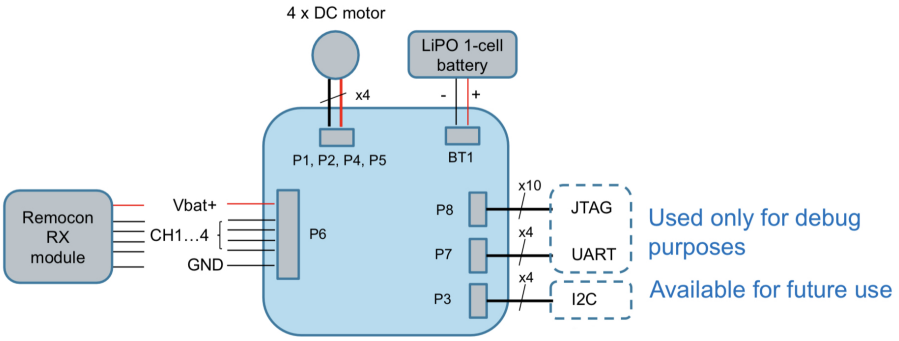

Figure 3.2.: Application connections on the FCU001V1 [17]

this project and can be freely assigned to new signals. The same applies for PB4, PB5, PA15 and PB14. In addition, PA9 and PA10 (UART[3]) are not required. Furthermore the pins at P3 configured for the I2C2 in Figure 3.2 can be remapped. The final mapping of the signals used in this project are discussed in Section 3.3.1.

3.1.2. FCU001V1 Software Description

The source code for the FCU001V1 can directly be downloaded from GitHub[4].
The basic firmware structure consists of the application, middleware and drivers level, see also Figure 3.4. The application level holds all functions that are developed for the user to control the flight: a remote control interface to interpret data commands from a remote control; a sensor management to retrieve sensor data; an attitude reference heading system (AHRS) to translate sensor data roll pitch and yaw anlges (quaternions); the flight control that combines the AHRS data with the data from the remote control to compute the flight strategy; a PID control to compute the required thrust for each motor.
The middleware handles the libraries to manage connectivity (USB and BLE). Lastly, the drivers manage the sensors and peripherals of the MCU.
The blocks "Utilities" and "CMSIS" in Figure 3.4 are functions that come from the STM32 architecture and corresponding ARM Cortex-M4[17].

A comprehensive overview of the software control flow is given in Figure 3.5, please refer to it for the following discussion.
Starting at the control inputs that are transmitted via BLE to the FCU, the system receives its target attitude, meaning specific values for roll, pitch, yaw and thrust. In the following these target values are referred to as setpoints. Apart from that, the actual value of above angles and thrust, the process-variables, are required. These are computed

[3] optional, can be used for debugging or datalogging
[4] `https://github.com/STMicroelectronics-CentralLabs/ST_Drone_FCU_F401`

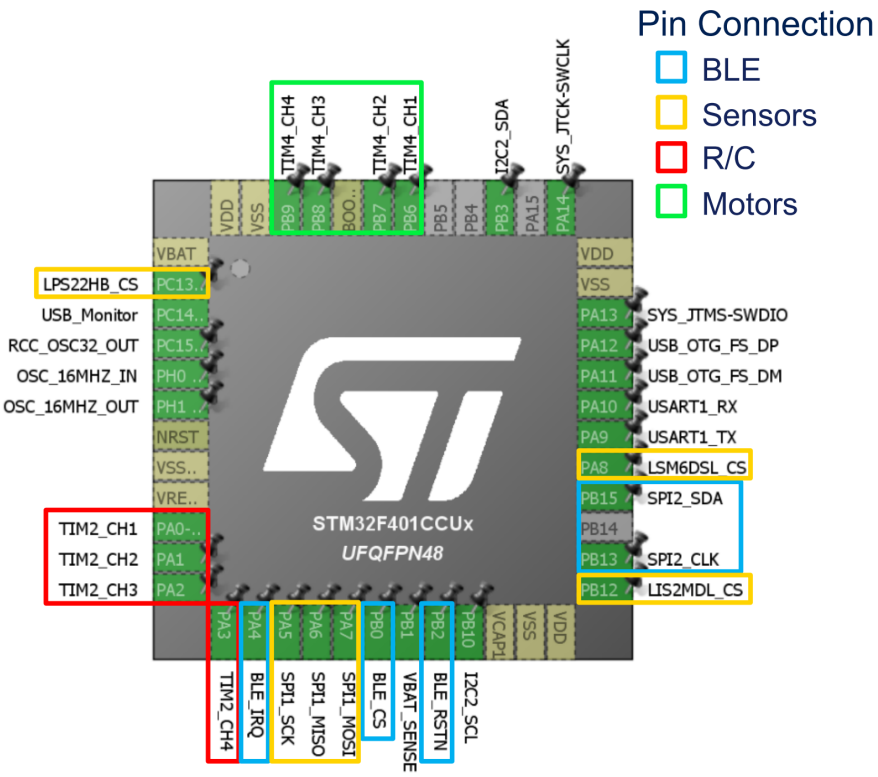

Figure 3.3.: STM32F401 connections [17]

as follows.
The raw data from the IMU is fed into the Attitude Heading Reference System (AHRS) algorithm. In order to run the PID stabilization algorithm, the data from the AHRS have to be translated to euler angles[5]. With the euler angles being our process Variable PV(t), the error term $e = setpoint - PV(t)$ can be computed. With the error term, the PID controller calculates the thrust to be applied to each motor such that the drone follows its setpoint.

3.2. DWM3000

The newly available DWM3000 module from Qorvo is based on their DW3110 UWB transceiver IC, see Figure 3.6a. It gives an easy access to the UWB technology by integrating the antenna, all RF circuitry, power management and clock circuitry in one module. It is compatible with TWR or TDoA systems to locate assets up to an accuracy of 10 cm thanks to its precise time stamping and message scheduling. The module powers a SPI interface to the host processor which runs all the applications (e.g. TWR);

[5] they describe the orientation of the drone

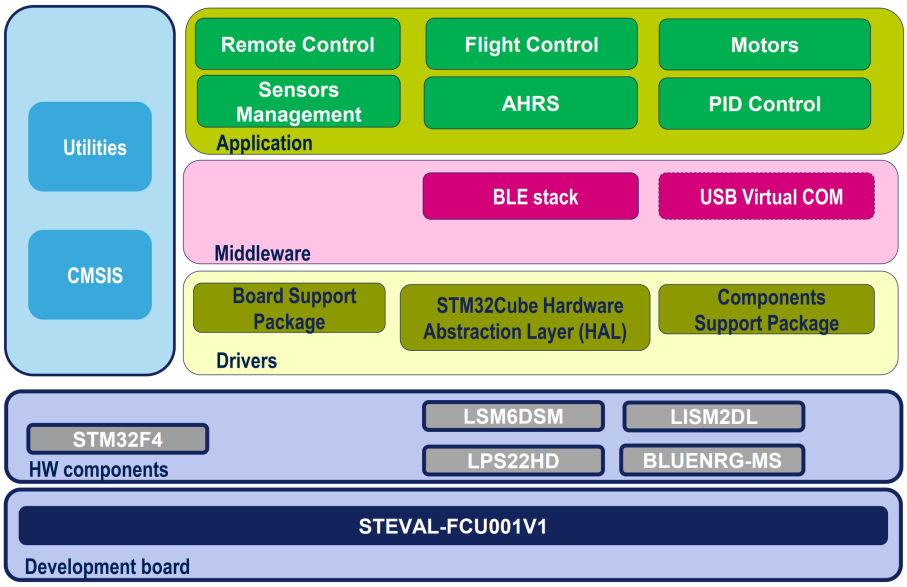

Figure 3.4.: Firmware architecture [17]

this interface is used to read and write to the registers in the DW3110 device. The SPI chip-select asserted to low by the host controller (master) marks the beginning of a transaction. All data and addresses are transferred as MSB first. The SPI MISO (master in slave out) needs to be configured as open drain when the SPI chip-select is deasserted. Furthermore, daisy chaining[6] is not supported. With its small footprint of 23 mm x 13 mm x 2.9 mm and a weight of less than 2 g it can be rapidly implemented in various systems [2].
Additionally, the lowered power consumption compared to its pin compatible predecessor increases battery lifetimes in mobile systems [23].

Despite the compact form factor, when being mounted on the application board one needs to carefully consider the proximity of the DWM3000 on-board ceramic monopole antenna to non-RF transparent materials. It is important that there is a keep-out area around the chip antenna of at least 1 cm radius, this can either be achieved by pointing the antenna off the board in free space or in a RF-transparent material (see [23] for details). In both cases the area of the application board should be flooded with ground copper.

Regarding the electrical specifications, the preliminary datasheet that was available at the time of this project, did not contain much information yet[7]. Therefore, the old

[6] MISO and MOSI lines are passed through a device when it is not chip selected
[7] i.e. no typical supply currents or gpio output current drives

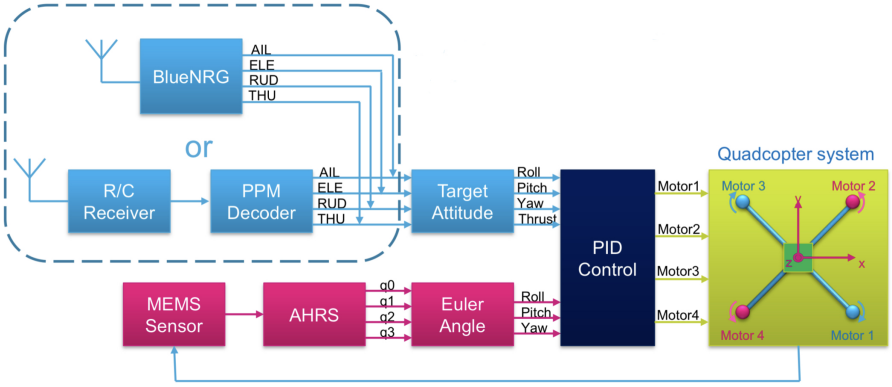

Figure 3.5.: Overall FW block diagram [17]

DWM1000's datasheet and the help of this work's experienced supervisors was taken into consideration to estimate maximum current ratings.
"The DWM3000 provides 8 configurable pins. On reset, all GPIO pins default to input. GPIO inputs, when appropriately configured, are capable of generating interrupts to the host processor via the IRQ signal. See DW3000 datasheet and DW3000 user manual provide full details of the configuration and use of the GPIO lines" [23].

3.3. PCB Design

The design of a shield for the FCU001V1 to connect it with the DWM3000 module was the main focus of this project.
When studying the FCU and the DWM3000, the required signals for the PCB have been worked out. After that, the different stackup options were considered, succeeded by the component selection. At this point, the tracks between the components had to be laid out. Lastly, all the circuitry was fitted on a board with specified shape for the Steval-Drone.
The following sections, discussing the points mentioned above in more detail, are arranged in the same order as explained above.
A high level block diagram of the DWM3000 shield connected to the FCU001V1 can be seen in Figure 3.7. All its parts are going to be discussed in the following. Note that for the complete schematic diagram, refer to Appendix A.

3.3.1. Required Signals and Connections

Firstly, it is important that the drone is able to fly and perform TWR exchanges at the same time. This implies that the provided flight controller software must not interfere with the connected shield and its connections to the host controller. As a result, only

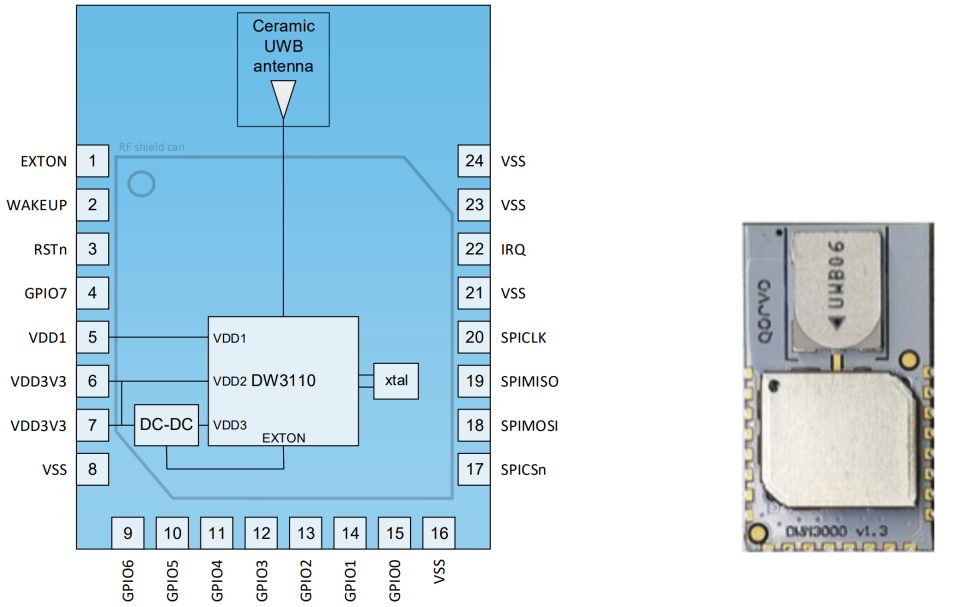

(a) Functional block diagram

(b) DWM3000 module

Figure 3.6.: The DWM3000 [24]

signals/pins that are not used by the flight controller can be used to connect the shield. In Section 5.2 of the DWM3000 datasheet [23] there is the most simple application diagram for the module depicted. This circuit diagram does integrate the DWM3000 by powering the device and connecting it to a host controller. Apart from the supply, the following connections have to be made.

For the communication with the host controller a 4-wire SPI interface is required, see Section 3.2 or the datasheet [23] for details.

In addition to this, two lines, a reset and an interrupt, are implemented. The former is active-low and used to reset all IC configurations back to default; it should never be driven high. The reset signal has to be driven low for at least 10 ns to function properly and then be left in open-drain mode. The DWM3000 has multiple interrupt events that can drive its IRQ output pin. It is an active high signal by default.

While this concludes all the signals required by the example from the datasheet, in this project there are some additional connections implemented.

Starting with two low current LEDs[8] connected to Pin 12 and 13 respectively. These have the purpose of supporting the debugging through visual feedback.

Lastly, to be able to turn off the DWM3000, the shutdown mode of the LP3982 LDO is used. As a result, the average power consumption can be decreased by shutting down the PCB shield. See Section 4.1 for the findings with respect to the power consumption. Note that the shutdown mode is enabled when pulled low[9]. The signals/connections that

[8] Vishay TLMS1000-GS08 and TLMY1000-GS08

[9] it is an active low signal

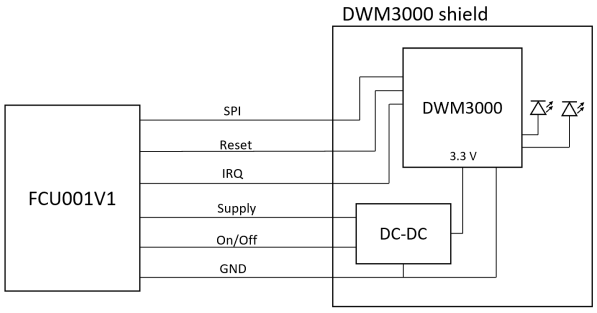

Figure 3.7.: High level block diagram of the PCB shield connected to the FCU

have to be mapped to the custom shield are the following.

- Supply Voltage (VBat+) and Ground (GND)
- 4 SPI lines
- A reset line
- 1 interrupt line
- 1 ON/OFF signal to control the onboard voltage regulator

With the datasheet of the STM32F401 and the data brief of the FCU001V1, the alternative functions of pins were investigated used to remap all the required signals. In table 3.1 are the required signals and their corresponding GPIOs and physical pins on the FCU001V1 board, see Figure 3.8.

Connections/Signals to custom PCB	used GPIOs of STM32F401 MCU	physical pins on the FCU001V1
VBAT+ (Supply Voltage)	na	P6, pin 1 (VBAT+)
SPI MOSI	PB5	LD1 (LED needs to be removed)
SPI MISO	PB4	LD2 (LED needs to be removed)
SPI CLK	PB3	P3 pin 2
DW NSS (SPI CSn)	PB10	P6, pin 4
DW IRQn	PA10	P7, pin 3
DW RESET	PA9	P7, pin 4
GND	na	P3, pin 4
ON/OFF	PA1	P6, pin 3

Table 3.1.: Required connections

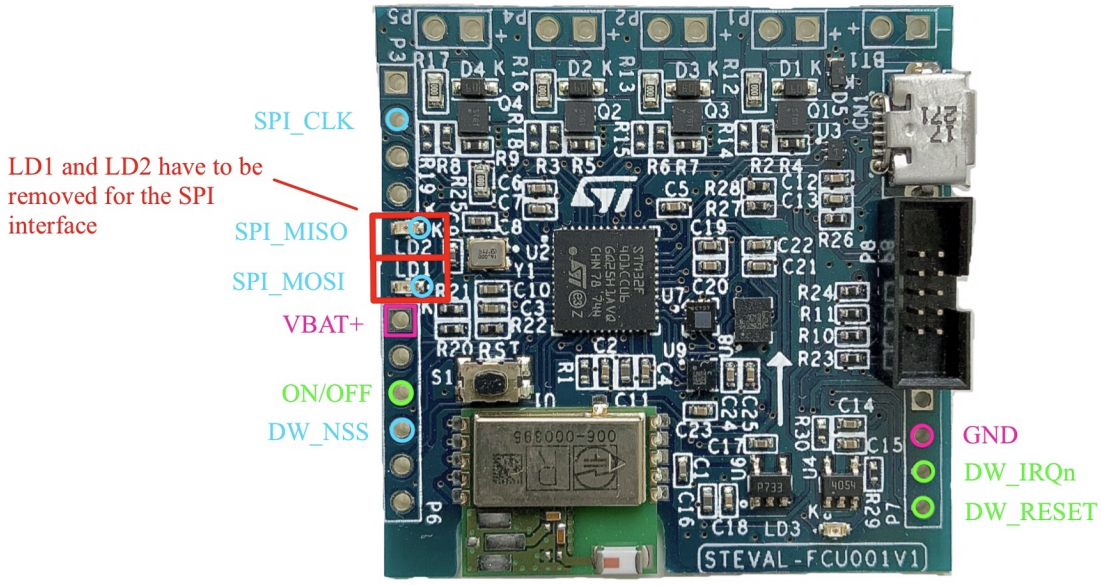

Figure 3.8.: FCU001V1 signal connections

For the MISO and MOSI, the LEDs LD1 and LD2 had to be removed, since there was no alternative found, see Table 3.1 and Figure 3.8.

3.3.2. Stackup

To meet the lighter weight from the requirements listed in 1.4 while also keeping as many rules as possible standard to keep the cost low, the design rules for this project were chosen to be as follows. A common double-sided PCB with total thickness of 1.6 mm seemed to be too heavy, for that reason 50 % thinner design was favored; with 0.8 mm overall thickness it was possible to reduce the weight while still keeping it relatively easy to solder components. The idea behind this is that an even thinner board of 0.4 mm for instance would have transferred heat too quickly to the other side of the board during soldering which could potentially reflow the solder an thus, detach components. As indicated, components where mounted on both sides of the PCB to reduce the space needed.
The minimal limits for electrical clearance, track width and annular rings where set to 0.15 mm and for drill holes 0.3 mm.
The copper thickness in the top and bottom layer was set to 35 μm and the dielectric is standard FR-4[10].

[10]FR-4 is a standard for a glass-reinforced epoxy resin laminate, 'FR' stands for flame retardant

#	Name	Material	Type	Weight	Thickness
	Top Overlay		Overlay		
	Top Solder	Solder Resist	Solder Mask		0.01016mm
1	Top Layer		Signal	1oz	0.03556mm
	Dielectric 1	FR-4	Dielectric		0.708mm
2	Bottom Layer		Signal	1oz	0.03556mm
	Bottom Solder	Solder Resist	Solder Mask		0.01016mm
	Bottom Overlay		Overlay		

Figure 3.9.: DWM3000 Shield Layer Stackup

3.3.3. Components

In this project, apart from the DWM3000 module, SMD resistors, capacitors and LEDs of the 0603 package were used. And furthermore, the voltage regulator was in the VSSOP-8 package.

Passive Components

The resistors R1 and R2 are used to limit the current through the LEDs DS1 and DS2. Since a SPI communication is working in the lower MHz regime, it can be assumed that there are no high frequency effects (reflection, over- and undershoot). Nevertheless, a short rise time causes sharp edges which can lead to HF problems. Resistors R4 to R7 are to smooth out the transients coming from the sharp edges. The resistor values where taken from the DWS3000 schematic[11].
Resistors R8 and R3 were taken from the datasheets of the LP3982 and DWM3000 respectively.
The capacitors all act as bypass capacitors that smooth out the supply voltages[12].

Active Components

Besides the passive components, the design has two LEDs connected to DWM3000 Pins 12 and 13, following the DWS3000 schematic. According to the datasheet of the DWM3000 pin 12 can be configured for use as a TXLED driving pin that can be used to light a LED following a transmission. Similarly, pin 13 can be configured for use as a RXLED driving pin that can be used to light a LED during receive mode [23].

The other active component is a Low Dropout regulator (LDO), the LP3982 Ultra-Low-Dropout, Low-Noise CMOS Regulator, see [25]. The version that is used in this project is one with a fixed 3.3 V output voltage[13]. This LDO is used because of its output current of up to 300 mA that provides a large enough margin since electrical specifications

[11] `https://www.decawave.com/wp-content/uploads/2020/04/DWS1000_Schematics_V1_2.pdf`
[12] values according to datasheets of the DWM3000 and the LP3982
[13] 3.3 V is the input voltage the DWM3000 requires

are not yet available on the datasheet. Furthermore, the device offers very stable and precise output voltage[14] which is very beneficial considering the noisy environment of the application on the drone. Also the supply current of typically only 1 nA during shutdown mode is well suited for this project where a low power consumption is highly important. In addition to this, a dropout voltage of 40 mV at 100 mA load current allows for good utilization of the battery's capacity as it gets closer to its end-of-life voltage[25], beyond 80% discharge capacity (see Figure 3.10) and thus makes it suited for battery-powered applications.

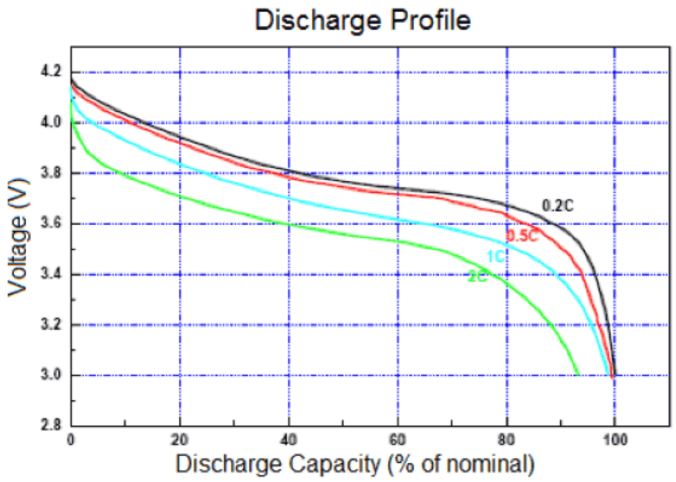

Figure 3.10.: Discharge profile of a typical LiPo battery: 3.0 V cutoff at room temperature [26]

3.3.4. Track Widths

A PCB track width calculator [15] was used to estimate the required trace width. The minimum required trace width for the maximum current of 300 mA that the LDO can deliver is at 0.03 mm. Since thicker tracks reduce resistance and the lower limit set by the manufacturer is at 0.15 mm, the width for the supply (VBAT+), the output of the LDO and ground (GND) was set to 0.3 mm. For the rest of the signals 0.15 mm were chosen because there are smaller currents.

[14] +- 2% voltage tolerance
[15] `https://www.4pcb.com/trace-width-calculator.html`

3.3.5. Outline and Dimensions

The shape and outline of the PCB was restricted by the layout guidelines[16] and the drone frame onto which it will be mounted. The components are mounted on the top and bottom layer for this purpose. The shield can either be mounted with screws onto the frame as it is depicted in Figure 3.12. Note that for the final application, the 10-pin header is being removed and the wires are soldered directly onto the board. The headers purpose is to provide more flexibility during debugging.

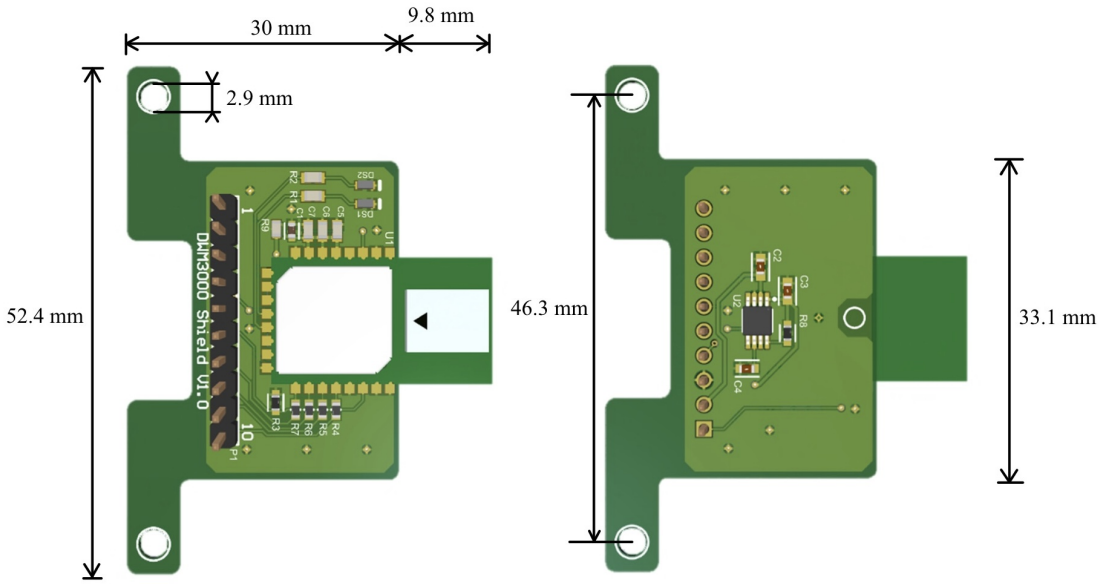

Figure 3.11.: DWM3000 Shield Dimensions

3.3.6. The DWM3000 Shield connected to the Flight Control Unit

In the following two sections, it is discussed how the custom shield is connected to the FCU001V1 from the hardware and software perspective.

Hardware-related

As one can see in Figure 3.11, the shield's dimensions are specially designed such that it can be attached to the drone frame as shown with the 3D model depicted in Figure 3.12. Please note that the 10-pin header is not intended to be attached in this final application; cables are rather soldered directly to their pads. Also the user has the choice between screws or other adhesives to attach the shield to the frame from which the latter is

[16] DWM3000 datasheet, Section 5.1

suggested to reduce the weight.
Note that in the 3D model it is clearly visible that the keep-out area discussed in Section 3.2 was taken into account. More precisely, by positioning the chip antenna in free space, away from the application board and the FCU which is mounted on the bottom side of the square platform, there are no RF-blocking obstacles around it.

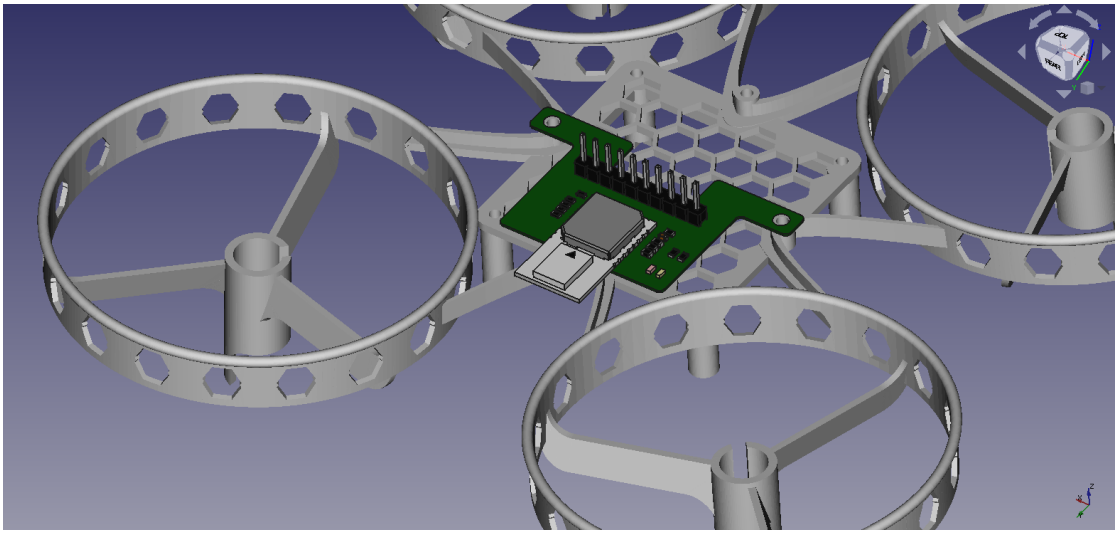

Figure 3.12.: DWM3000 Shield mounted on the drone

Software-related

The goal here was to have the TWR sample code running on the FCU while also allowing it to run the flight control sample code provided by STMicroelectronis alongside. The latter can be run out-of-the-box whereas for the TWR some changes had to be applied. As the DW3000 API Guide [17] provides example codes for the user to discover the module's capabilities, the included TWR code example was used to verify that the shield is working properly.
The C source code for the TWR is created for the ST NUCLEO-F429ZI development board based on STM32Cube. Hence, it had to be partly rewritten to be able to run on the STM32F401 MCU in the FCU. The adjustments involved the creation of an SPI interface and the configuration of the required GPIOs as depicted in table 3.1. For the SPI, the basic parameters are the Motorola frame format with a data size of 8 Bits, MSB first. The clock Parameters require a baud rate of 2.25 MBit/s and clock polarity set low.
The extra signal line handling the WakeUp of the DW3000 IC is not present on the custom shield. However, the host controller can also wake up the IC by pulling the SPI

[17] Link

chip select line low for > 500 μs [27]. The corresponding adjustment in the source code had to be made in the file `port.h`.
In the rest of the code all the commands to print out some strings to a serial terminal were removed since this function is not available on the FCU001V1 (UART pins are remapped).
If the frequency of the TWR exchanges has to be changed, this can be done via the parameter RNG_DELAY_MS which is the Inter-ranging delay period in miliseconds.

Above described adaptions to the original TWR code led to the system flow as described in the following.
To begin, see Figure 3.13 for a high level overview of the software run on the FCU001V1. In this scenario, the drone is the initiator of the TWR exchange. After starting up the FCU, the DWM3000 starts up too as soon as a stable power supply is applied. The software then checks whether the DWM3000 is in IDLE or not; if not, the startup procedure has to be started again. Otherwise, it checks if the PLL and RX calibration was successful, if this is not the case, the host can reset the device or the whole startup can be repeated.
Once the DWM3000 is in IDLE and configured properly, the initiator initiates an exchange by sending a "poll". The device is waiting/listening for a repsonse upon a timeout time has passed. The timeout allows the receiver to stop listening in situations where the responder is out of range or did not receive the message to respond to.
When the expected response fram is received, the initiator retrieves poll transmission and response reception timestamps and computes the final message transmission time. All timestamps are written in the final message which is then sent to the responder. After a pre-programmed ranging delay the initiator sends a "poll" again.

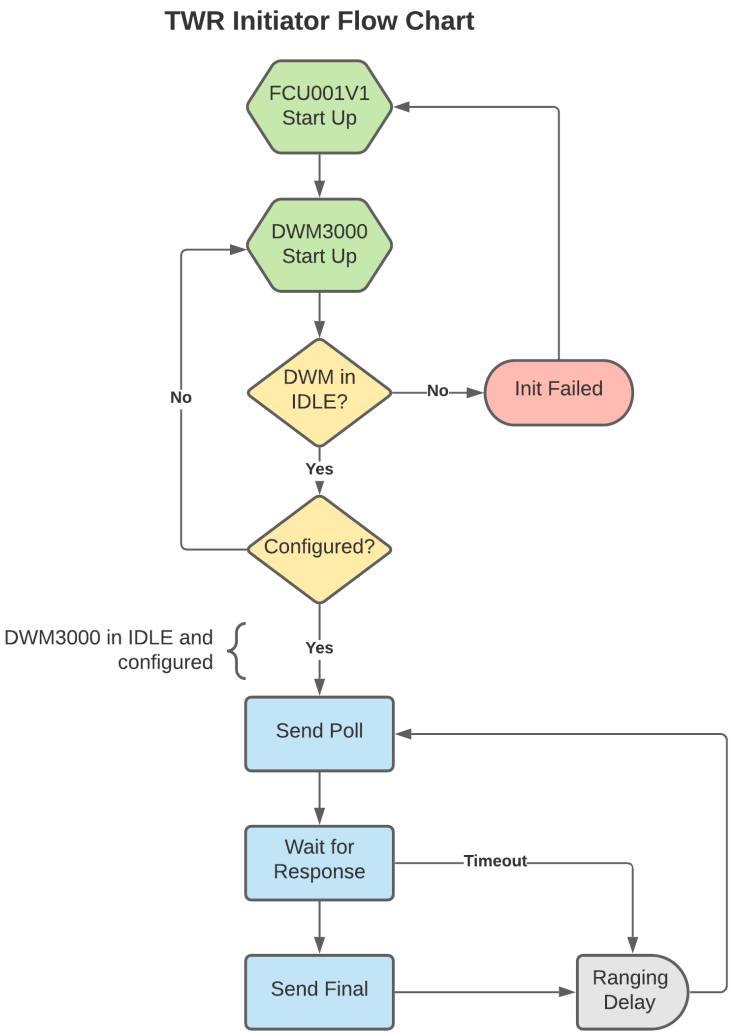

Figure 3.13.: Flow Chart for TWR system start up

Chapter 4

Results

In the end, what matters is that the DWM3000 module is functioning and ready for TWR. This chapter is structured in the sections 'Power consumption' and 'Pin configurations and Specifications' of the final PCB.
Since the verification of the accuracy of the distance measurements made in this framework was not of interest, the final evaluation is limited to the fact that the measurement function is ensured. Furthermore, the power consumption and general specifications have been elaborated.

The results in terms of written SW and Altium Designer documentation is accessible on GitLab[1].

4.1. Power Consumption

On micro-drones, there is a very limited power budget, thus for exact flight planning the power consumption of the PCB Shield is of interest. The following measurement was taken with the DWM3000 configured as the initiator [2].

[1] Altium Project Data: `https://git.ee.ethz.ch/pbl/sf2021/yanickbuchel/-/tree/master/PCB_Design/Altium%20Project<%20Data/PCB_DWM3000` Software: `https://git.ee.ethz.ch/pbl/sf2021/yanickbuchel/-/tree/master/Software`

[2] This is the configuration which the DWM3000 on the drone will usually be in

4.1.1. Measurement

Initially, the measurement of the power consumption was performed with the N6705C DC Power Analyzer. For this purpose, the cables 'Supply' and 'GND' [3] where connected to the power source. However, the measurement was very noisy and the sampling time was not short enough for a sufficiently precise measurement.
The measurement had to be performed with an oscilloscope [4]. Using a shunt 10.0 Ω resistor and 4.2 V applied to the Supply[5].

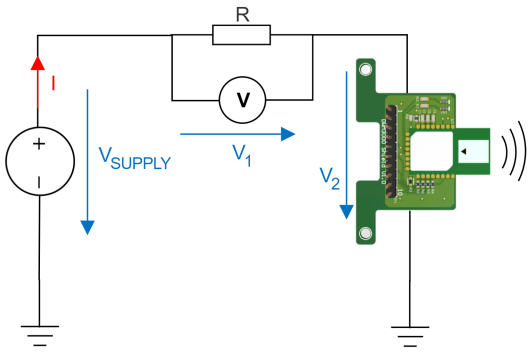

Figure 4.1.: Power Consumption Measurement Setup

From the measurement setup in Figure 4.1, we can calculate the consumed power as follows.

$$I = \frac{V_1}{R} \tag{4.1}$$

$$V_2 = V_{SUPPLY} - V_1 \tag{4.2}$$

$$P = V_2 \cdot I \tag{4.3}$$

TWR mode

With this simple calculation the graph as shown in Figure 4.2 is obtained (unfiltered power consumption). However, the measurement was very noisy, to get rid of the noise, a Butterworth low-pass filter was applied. For a sample period of 2 ms and a sample rate of 400 kHz the cutoff frequency of the low-pass filter was set to 10 kHz as it provided the best results which are seen Figure 4.2.
The graph of the power consumption clearly shows three peaks which are an indicating the three exchanged frames within a TWR measurement. As this is representing the

[3] Pins 2 and 3 on the DWM3000 Shield
[4] Sampling time: 2.5 μs
[5] Pin 2

power consumption of an initiator, the first increase corresponds to the 'poll', the second to the 'response' and the third to the 'final' message being sent. It can further be concluded that a TX event[6] consumes up to 152 mW whereas the RX event consumes 23.0 % more with an absolute value of 187 mW. The total time of such an exchange is 2 ms and the average power during this period is 78.6 mW, denoted as 'average power' in Figure 4.2. The other measure of interest is the power consumption while the module is waiting for the next TWR exchange. During this period, the average power consumption is 48.7 mW.

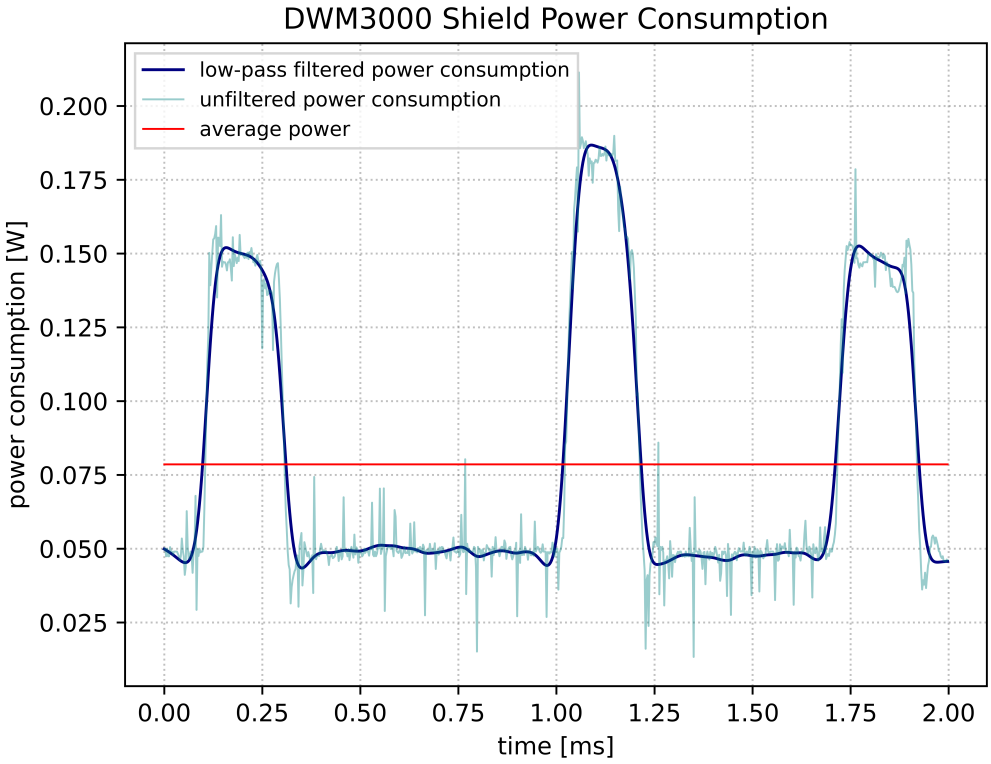

Figure 4.2.: Measured Power Consumption of a single TWR exchange

Since one ranging exchange takes approximately 2 ms, we can estimate the power consumption for various ranging frequencies of up to 500 Hz. In theory, it is even possible to further decrease the 2 ms, since the time between the frames can be adjusted as well. As 500 Hz is already more than one needs for the purpose of the application in this project, a further increase in ranging frequency is not in the scope of this work anymore.
In table 4.1 is the estimated power consumption at different frequencies depicted. With the average power of one exchange $p_{avg,burst} = 78.6$ mW and the power when waiting

[6] represented by the first and third peak

for an exchange $p_{avg,IDLE} = 48.7$ mW known, the average power consumption p_{avg} can easily be estimated. The formula to calculate the latter is

$$p_{avg} = \frac{1000 - T_{burst} \cdot f_{ranging} \cdot p_{avg,IDLE} + T_{burst} \cdot f_{ranging} \cdot p_{avg,burst}}{1000} \tag{4.4}$$

frequency [Hz]	p_{avg} [mW]
10	49.30
20	49.90
50	51.69
100	54.68
150	57.67
200	60.66
400	72.62

Table 4.1.: Power Estimates for different ranging frequencies (Shutdown of the LP3982 not used)

Shutdown Mode

When the Signal ON/OFF on Pin 4 of the DWM3000 Shield is pulled to GND, the on board voltage regulator is turned off, meaning that its output voltage is zero. The power consumption measured in this case is negligibly small, with a current draw of less than 0.01 μA it was not possible for the used test equipment to detect any current. In fact, the datasheet of the LP3982 confirms that the typical value for the shutdown supply current is 0.001 μA [25].

4.1.2. Periodic Shutdown

Apart from the above ranging scheme where the DWM3000 module is in an IDLE state in between actual ranging exchanges where it still consumes approximately $p_{avg,IDLE} = 48.7$ mW, this work proposes another more power efficient method.
The ON/OFF signal that allows the host controller to let the LP3982 LDO go into shutdown mode, where it only draws a supply current of $I_{Shutdown} = 1$ nA. With a fully charged battery (VBAT+ = 4.2 V) the power $p = I_{Shutdown} \cdot VBAT+$ is in the low nW range and thus can be neglected.
To estimate the power consumed when this feature is used, the required power up time of both the LP3982 and the DWM3000 have to be known. In the DW3000 API Guide

and the drivers[7] provided along with it, it says in the source code of example 5a, ds_twr_initiator.c,that the DW3000 IC needs 2 ms to start up. In comparison, the LP3982 has a rather short start-up time of 120 μs. Theoretically, the system start up needs around 2.12 ms until it is ready for TWR exchanges. To make this principle work, we need to turn the LDO back on at least the 2.12 ms + some margin[8] before the next ranging exchange happens.

4.2. DWM3000 Shield Specifications

Pin Configurations

The DWM3000 Shield pin assignments are as shown in Figure 4.3 (top view).

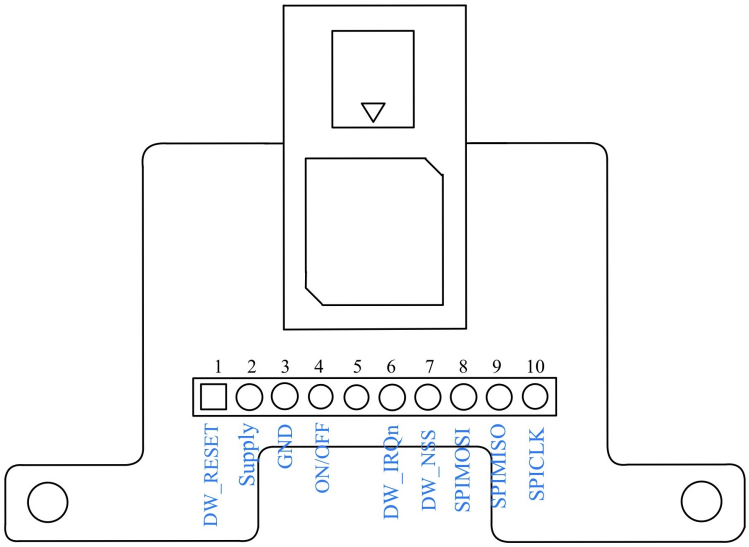

Figure 4.3.: DWM3000 Shield Pin Diagram

As one can see, the pins are numbered from 1 to 10. Their corresponding description can be found in Table 4.2. Note that pin 5 is not connected.

[7]The device driver is provided as source code to allow it to be ported to any target microprocessor system with an SPI interface

[8]to be determined

NAME	PIN	I/O	DESCRIPTION
DW_RESET	1	output	Reset signal for the DWM3000. Active Low Output. May be pulled low by external open drain driver to reset the DWM3000
Supply	2	input	Input supply voltage
GND	3	GROUND	Ground
ON/OFF	4	input	ON/OFF Signal for on-board voltage regulator. Active high.
-	5	-	-
DW_IRQn	6	output	Interrupt request from the DWM3000 to the host processor. Active high output.
DW_NSS	7	input	SPI chip select. Active low input. High-to-low transition starts a SPI transaction.
SPIMOSI	8	input	SPI data input
SPIMISO	9	output	SPI data output
SPICLK	10	input	SPI clock

Table 4.2.: DWM3000 Shield pin functions

Specifications

Table 4.3 shows the electrical specifications of the DWM3000 Shield. For the typical current for a transmission (TX) and a reception (RX) of a frame, the values were calculated as follows.

$$V_{2,TX/RX} = V_{SUPPLY} - V_{1,TX/RX} \tag{4.5}$$

The voltage $V_{1,TX/RX}$ is the measured voltage over the resistor which is know at the point of a TX or RX event, for the measurement setup refer to Figure 4.1. Also the power that the module is consuming during such an event is known from equation 4.3 such that it is possible to compute the current as:

$$I_{peak} = \frac{P_{TX/RX}}{V_{2,TX/RX}} \tag{4.6}$$

This result matches the measured values obtained with the DC Power Analyzer which was directly connected to the DWM3000 Shield; where current values of 50 mA for RX and 40 mA for TX were observed.

Parameter	Min.	Typ.	Max.	Unit	Note
Supply voltage	3.3	3.4 - 4.2	6	V	typical voltage range of LiPo battery
Supply current (DWM3000 in IDLE)		12.3		mA	
Supply current Shut-down		1		nA	
TX		40.0		mA	Ch 5, Supply = 3.8 V
RX		50.5		mA	Ch 5, Supply = 3.7 V
Logic Level		3.3		V	

Table 4.3.: DWM3000 Shield Electrical Specifications DC (at room temperature)

Chapter 5

Conclusion and Future Work

This thesis shows that a custom PCB that allows connection between the novel DWM3000 module and the FCU001V1 flight control unit was developed.
During the development of the PCB, particular focus was placed on a low overall weight in order to minimize the additional thrust required from the motors. Considering the high noise level expected which is caused by the motor currents, bypass capacitors were used to guarantee a stable supply voltage. For the same reason, an LDO was used for voltage regulation.
At this stage of progress, the developed shield is installed on the drone.
The next step could be first point-to-point distance measurements while flying prior to the development of a more complex system that allows real-time locating of the drone via triangulation.
The result of this work can also serve as a template for future projects that want to bring the UWB technology to their drones using the DWM3000. The past shows that the demand in this area is very high, note the previous work with the predecessor module DWM1000 (Section 2.4).

Appendix A

Schematic

The complete schematic of the DWM3000 Shield.

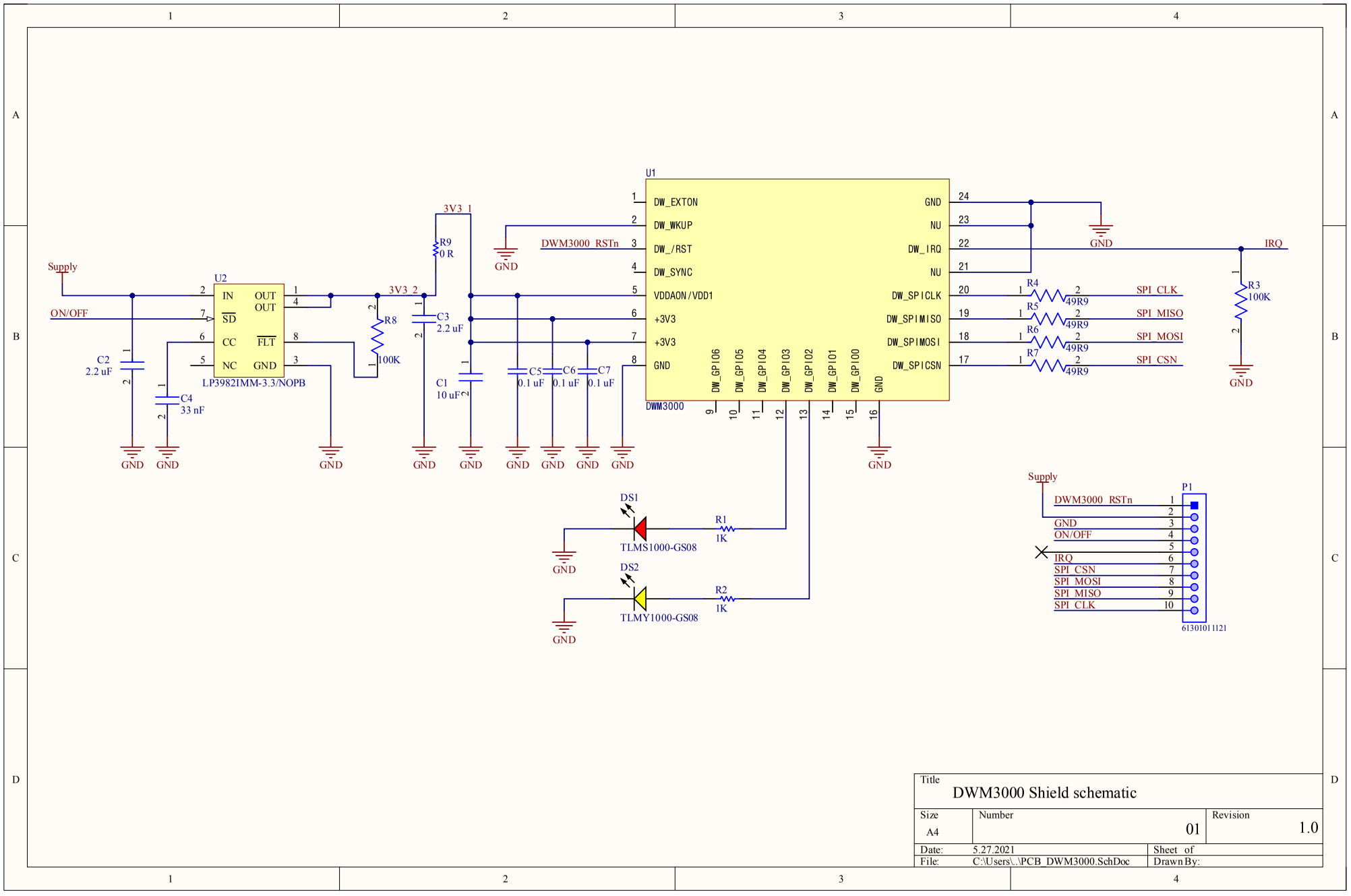
U1
DW_EXTON
DW_WKUP
DW_/RST
DW_SYNC
VDDAON/VDD1
+3V3
+3V3
GND
DW_GPIO6
DW_GPIO5
DW_GPIO4
DW_GPIO3
DW_GPIO2
DW_GPIO1
DW_GPIO0
GND
GND
NU
DW_IRQ
NU
DW_SPICLK
DW_SPIMISO
DW_SPIMOSI
DW_SPICSN
DWM3000
DWM3000_RSTn
3V3_1
3V3_2
R9
0 R
R8
100K
C3
2.2 uF
C1
10 uF
C5
0.1 uF
C6
0.1 uF
C7
0.1 uF
U2
IN
OUT
OUT
SD
CC
FLT
NC
GND
LP3982IMM-3.3/NOPB
Supply
ON/OFF
C2
2.2 uF
C4
33 nF
DS1
TLMS1000-GS08
DS2
TLMY1000-GS08
R1
1K
R2
1K
R4
R5
R6
R7
49R9
SPI_CLK
SPI_MISO
SPI_MOSI
SPI_CSN
IRQ
R3
100K
P1
GND
ON/OFF
SPI_CSN
SPI_MOSI
SPI_MISO
SPI_CLK
6130101121
Title
DWM3000 Shield schematic
Size
A4
Number
01
Revision
1.0
Date:
5.27.2021
Sheet of
File:
C:\Users\..\PCB_DWM3000.SchDoc
Drawn By:

Appendix B

Task Description

ETH
Eidgenössische Technische Hochschule Zürich
Swiss Federal Institute of Technology Zurich

Integrated Systems Laboratory
Project-Based Learning Center

Bachelor thesis at the
Department of Information Technology and
Electrical Engineering

for

Yanick Büchel

UWB for micro-drones

Advisors: Tommaso Polonelli
Michele Magno

Professor: Prof. Luca Benini

Handout Date: 01.03.2021
Due Date: 11.06.2021

1 Project Goals (15 weeks)

Nowadays, the industry is pushing the evolution of autonomous flying vehicles (UAV) toward rapidly decreasing form factors and increasing of computational capabilities. On the other hand, pioneering research has already demonstrated nano-scale aerial vehicles, i.e., pico-size UAVs. However, flight control, navigation, and planning capabilities are either absent or based on monocular low-resolution cameras. In contrast, relatively big-sized drones (i.e., DJI or Matek) have been proven capable of impressive autonomous sense-and-act capabilities, running in real-time complex and computationally intensive multi-sensor and vision-based control systems.

Therefore, this project focuses on this challenging class of Unmanned Autonomous Vehicles, characterized by few centimeters in diameter, tens of grams in weight, and a few Watts total power consumption, of which 85% is to be dedicated to the propellers, leaving a total power budget for onboard sensing, computation, control actuation of only a few hundred mW. Thus, in this project our nano-size UAVs is based on an STM microcontroller, specifically the STEVAL-FCU001V1 development board, which support custom firmware and hardware. This thesis focuses on enhancing the nano-drone capabilities by adding wireless connectivity and indoor positioning, through the DW3000, the state-of-the-art UWB transceiver.

2 Tasks

The project will be split into three phases, as described below:

Phase 1 (Weeks 1-5)

1. Investigate and study the state-of-the-art technology of UWB ranging and wireless communication.
2. Introduction to PCB design, Altium: schematics and layout;
3. Getting started with the STM32 environment, IDE, SDK, HAL, and cross compilation/programming;
4. Getting started with the STEVAL-FCU001V1 development board;
5. Running and debugging the STEVAL-FCU001V1 support firmware and the UAV control algorithms.

Phase 2 (weeks 5-12)

1. DW3000 schematic. Specific focus on integrating the PCB-shield with STEVAL-FCU001V1;
2. Shield Layout and PCB production;
3. Component soldering and logic/electrical assessment;
4. Functional test with STEVAL-FCU001V1 and the new custom DW3000 shield.

Phase 3 (last 2 weeks)

1. Finalizing the tests and optimizations on the final version
2. Write the final document and prepare a presentation.

3 Milestones

By the end of **Phase 1** the following should be completed:

- Good working experience with STEVAL-FCU001V1 and Altium Design;
- Advanced knowledge about the DW3000 transceiver (datasheet and application guides) and the STEVAL-FCU001V1 firmware.

By the end of **Phase 2** the following should be completed:

- Schematic and PCB layout;
- Production, assembly, testing, and assessment.

By the end of **Phase 3** the following should be completed:

- Practical functional verification;
- Final presentation;
- Final report, including final results;

4 Thesis Organization

The Bachelor's Thesis is the final part of the program and is usually carried out in the sixth semester. During the thesis, students will gain initial experience in the independent solution of a technical-scientific problem by applying the acquired specialist and social skills. The grade is based on the following: (i) Difficulty of the project; (ii) Student effort and learning curve; (iii) Results in terms of quality and quantity; (iv) final presentation; (v) documentation.

A Bachelor's Thesis should take about half of a student's time during one semester, i.e., about 300-400 hours. The thesis includes an oral presentation and a written report, and it is graded. Before starting, the project must be registered in myStudies ("Projects/papers/theses").

4.1 Weekly Report

Weekly meetings will be held between the student and the assistants. The exact time and location of these meetings will be determined within the first week of the project in order to fit the students and the assistants schedule. These meetings will be used to evaluate the status and progress of the project. Beside these regular meetings, additional meetings can be organized to address urgent issues as well. The report, along with all other relevant documents (source code, datasheets, papers, etc), should be uploaded to a clouding service.

4.2 Written report

Documentation is an important and often overlooked aspect of engineering. One final report has to be completed within this project. The common language of engineering is de facto English. Therefore, the final report of the work is preferred to be written in English. Any form of word processing software is allowed for writing the reports, nevertheless the use of LaTeX or any other vector drawing software (for block diagrams) is strongly encouraged by the IIS staff.

4.3 Final Presentations

At the end of the project, the outcome of the thesis will be presented through an oral presentation.

.

Appendix C

Declaration of Originality

Eidgenössische Technische Hochschule Zürich
Swiss Federal Institute of Technology Zurich

Declaration of originality

The signed declaration of originality is a component of every semester paper, Bachelor's thesis, Master's thesis and any other degree paper undertaken during the course of studies, including the respective electronic versions.

Lecturers may also require a declaration of originality for other written papers compiled for their courses.

I hereby confirm that I am the sole author of the written work here enclosed and that I have compiled it in my own words. Parts excepted are corrections of form and content by the supervisor.

Title of work (in block letters):

UWB for micro-drones

Authored by (in block letters):

For papers written by groups the names of all authors are required.

Name(s):	**First name(s):**
Büchel	Yanick

With my signature I confirm that

- I have committed none of the forms of plagiarism described in the 'Citation etiquette' information sheet.
- I have documented all methods, data and processes truthfully.
- I have not manipulated any data.
- I have mentioned all persons who were significant facilitators of the work.

I am aware that the work may be screened electronically for plagiarism.

Place, date	**Signature(s)**
11.06.2021	Y. Büchl

For papers written by groups the names of all authors are required. Their signatures collectively guarantee the entire content of the written paper.

List of Acronyms

AoA . . . . . Angle of Arrival

BLE . . . . . Bluetooth Low Energy

FCU . . . . . Flight Control Unit

IC . . . . . Integrated Circuit

LDO . . . . . Low Dropout regulator

MPC . . . . . Multipath Component

PCB . . . . . Printed Circuit Board

RSSI . . . . . Received Signal Strength Indicator

RTLS . . . . . Real Time Locating System

TDoA . . . . . Time Difference of Arrival

ToF . . . . . Time of Flight

TWR . . . . . Two-Way Ranging

UAV . . . . . Unmanned Aerial Vehicle

UWB . . . . . Ultra-Wideband

List of Figures

List of Tables

Bibliography

[1] bitcraze, "Loco Positioning system," 2021, [Online; accessed 07-June-2021]. [Online]. Available: https://www.bitcraze.io/documentation/system/positioning/loco-positioning-system/

[2] J. Tiemann, F. Schweikowski, and C. Wietfeld, "Design of an uwb indoor-positioning system for uav navigation in gnss-denied environments," in *2015 International Conference on Indoor Positioning and Indoor Navigation (IPIN)*, 2015, pp. 1–7.

[3] C. I. Inc., "Amazon's Jeff Bezos looks to the future," 2013, [Online; accessed 28-May-2021]. [Online]. Available: https://www.cbsnews.com/news/amazons-jeff-bezos-looks-to-the-future/

[4] T. Özaslan, K. Mohta, J. Keller, Y. Mulgaonkar, C. J. Taylor, V. Kumar, J. M. Wozencraft, and T. Hood, "Towards fully autonomous visual inspection of dark featureless dam penstocks using mavs," in *2016 IEEE/RSJ International Conference on Intelligent Robots and Systems (IROS)*, 2016, pp. 4998–5005.

[5] R. D'Andrea, "Guest editorial can drones deliver?" *IEEE Transactions on Automation Science and Engineering*, vol. 11, no. 3, pp. 647–648, 2014.

[6] infsoft, "Indoor positioning, tracking and indoor navigation with wi-fi," 2021, [Online; accessed 14-May-2021]. [Online]. Available: https://www.infsoft.com/technology/positioning-technologies/wi-fi

[7] ——, "Using beacons for indoor positioning, tracking and indoor navigation," 2021, [Online; accessed 14-May-2021]. [Online]. Available: https://www.infsoft.com/technology/positioning-technologies/bluetooth-low-energy-beacons

[8] M. Malajner, P. Planinsic, and D. Gleich, "UWB Ranging Accuracy."

[9] Z. Sahinoglu, S. Gezici, and I. Güvenc, *Ultra-wideband signals*. Cambridge University Press, 2008, p. 20–43.

[10] ——, *Introduction*. Cambridge University Press, 2008, p. 1–19.

[11] D. Neirynck, E. Luk, and M. McLaughlin, "An alternative double-sided two-way ranging method," in *2016 13th Workshop on Positioning, Navigation and Communications (WPNC)*, 2016, pp. 1–4.

[12] S. Lupashin, M. Hehn, M. W. Mueller, A. P. Schoellig, M. Sherback, and R. D'Andrea, "A platform for aerial robotics research and demonstration: The flying machine arena," *Mechatronics*, vol. 24, no. 1, pp. 41–54, 2014. [Online]. Available: https://www.sciencedirect.com/science/article/pii/S0957415813002262

[13] Z. Sahinoglu, S. Gezici, and I. Güvenc, *Position estimation techniques.* Cambridge University Press, 2008, p. 63–100.

[14] *APS013 APPLICATION NOTE, The implementation of two-way ranging with the DWM1000*, Decawave, 2015, Rev. 2.3.

[15] Z. Sahinoglu, S. Gezici, and I. Güvenc, *Ranging protocols.* Cambridge University Press, 2008, p. 148–180.

[16] T. Polonelli, Y. Qin, E. M. Yeatman, L. Benini, and D. Boyle, "A flexible, low-power platform for uav-based data collection from remote sensors," *IEEE Access*, vol. 8, pp. 164 775–164 785, 2020.

[17] A. Basile, "Getting started with st drone kit," https://www.st.com/content/ccc/resource/sales_and_marketing/presentation/product_presentation/group0/bd/cc/11/15/14/d4/4a/85/STEVAL-DRONE01_GETTING_STARTED_GUIDE/files/steval-drone01_getting_started_guide.pdf/jcr:content/translations/en.steval-drone01_getting_started_guide.pdf, feb 2020, online; accessed 27-May-2021.

[18] O. Liang, "EVERYTHING ABOUT LIPO BATTERY FOR RACING DRONES," may 2019, [Online; accessed 28-May-2021]. [Online]. Available: https://oscarliang.com/lipo-battery-guide/

[19] Pcbcart, "Layer Stackup," na, [Online; accessed 27-May-2021]. [Online]. Available: https://www.pcbcart.com/pcb-capability/layer-stackup.html

[20] D. P. Vlad Niculescu, Michele Magno and L. Benini, "An energy-efficient localization system for imprecisely positioned sensor nodes with flying uavs," 2020.

[21] S. Li, M. Coppola, C. De Wagter, and G. Croon, "An autonomous swarm of micro flying robots with range-based relative localization," 03 2020.

[22] W. Chantaweesomboon, C. Suwatthikul, S. Manatrinon, K. Athikulwongse, K. Kaemarungsi, R. Ranron, and P. Suksompong, "On Performance Study of UWB Real Time Locating System."

[23] *DWM3000 IEEE 802.15.4-z UWB Transeiver Module*, qorvo, Nov. 2020, Rev. 0.1 Preliminary version.

[24] *DWM3000 Product Brief*, Qorvo, apr 2021, Rev. A.

[25] *LP3982 Micropower, Ultra-Low-Dropout, Low-Noise, 300-mA CMOS Regulator*, Texas Instruments, apr 2017, Revised April 2017.

[26] adafruit, "Li-Ion & LiPoly Batteries," 2012, [Online; accessed 27-May-2021]. [Online]. Available: https://learn.adafruit.com/li-ion-and-lipoly-batteries/voltages

[27] *DW3000 DEVICE DRIVER APPLICATION PROGRAMMING INTERFACE (API) GUIDE*, Decawave, jul 2020, Version 1.4.

[28] J. Kulmer, S. Hinteregger, B. Grosswindhager, M. Rath, M. S. Bakr, E. Leitinger, and K. Witrisal, "Using DecaWave UWB Transceivers for High-accuracy Multipath-assisted Indoor Positioning."

[29] Y. Chen and H. Kobayashi, "Signal strength based indoor geolocation."

[30] *PRODUCT BRIEF: DWM3000*, qorvo, 2020, Version 1.1.

[31] M. W. Mueller, M. Hamer, and R. D'Andrea, "Fusing ultra-wideband range measurements with accelerometers and rate gyroscopes for quadrocopter state estimation," in *2015 IEEE International Conference on Robotics and Automation (ICRA)*, 2015, pp. 1730–1736.

[32] A. Ledergerber and R. D'andrea, "Calibrating away inaccuracies in ultra wideband range measurements: A maximum likelihood approach," *IEEE Access*, vol. 6, pp. 78 719–78 730, 2018.

[33] S. Weiss, M. W. Achtelik, S. Lynen, M. C. Achtelik, L. Kneip, M. Chli, and R. Siegwart, "Monocular vision for long-term micro aerial vehicle state estimation: A compendium," *Journal of Field Robotics*, vol. 30, no. 5, pp. 803–831, 2013. [Online]. Available: https://onlinelibrary.wiley.com/doi/abs/10.1002/rob.21466

[34] Xilinx. (2011, Nov.) Virtex-6 FPGA Configuration - User Guide. UG360 (v3.4) November 18, 2011. [Online]. Available: http://www.xilinx.com/support/documentation/user_guides/ug360.pdf

[35] Wikipedia, "Wi-fi positioning system — wikipedia, the free encyclopedia," 2021, [Online; accessed 14-May-2021]. [Online]. Available: https://en.wikipedia.org/wiki/Wi-Fi_positioning_system